Cancer Research

Intravital FLIM-FRET imaging reveals dasatinibinduced spatial control of Src in pancreatic cancer.

Max Nobis, Ewan J Mcghee, Jennifer P. Morton, et al.

Cancer Res Published OnlineFirst June 7, 2013.

Intravital FLIM-FRET imaging reveals dasatinib-induced spatial control of Src in pancreatic cancer

Max Nobis[1], Ewan J. McGhee[1], Jennifer P. Morton[1], Juliane P. Schwarz[1], Saadia A. Karim[1], Jean Quinn[2], Mike Edward[2], Andrew D. Campbell[1], Lynn C. McGarry[1], T.R. Jeffry Evans[1], Valerie G. Brunton[3], Margaret C. Frame[3], Neil O. Carragher[3], Yingxiao Wang[4], Owen J. Sansom[1], Paul Timpson[#1,5] and Kurt I. Anderson[#1].

[1]The Beatson Institute for Cancer Research, Garscube Estate, Glasgow, G61 1BD, UK
[2]Section of Dermatology, School of Medicine, University of Glasgow, UK
[3]Edinburgh Cancer Research Centre, Institute of Genetics and Molecular Medicine, University of Edinburgh, Edinburgh, EH4 2XR, UK
[4]Department of Bioengineering, University of Illinois, Urbana-Champaign, USA
[5]The Garvan Institute of Medical Research and The Kinghorn Cancer Centre, 370, Victoria St, Darlinghurst, Sydney, NSW, 2010, Australia.

Running title: Imaging drug targeting in live tumors.

Key words: Intravital imaging, FLIM, FRET, Src, adhesion & migration, invasion & metastasis

Abbreviations: ECM, extracellular matrix; FLIM, fluorescence lifetime imaging microscopy; FRET, fluorescence resonance energy transfer; FRAP, fluorescence recovery after photobleaching; PDAC, pancreatic ductal adenocarcinomas; SHG, second harmonic generation; GLCM, grey-level co-occurrence matrix and TCSPC, time correlated single photon counting

Conflict of interest: the authors have no conflict of interest.
Word Count: 5000
Figures: 7

[#] Authors for Correspondence;
Dr Paul Timpson
The Garvan institute of Medical Research & Kinghorn Cancer Centre, 370, Victoria st, Darlinghurst, NSW 2010, Australia.
Email: p.timpson@garvan.org.au Tel +61 2 9355 5821
Prof Kurt I. Anderson
The Beatson Institute for Cancer Research, Garscube Estate, Glasgow, G61 1BD, UK
Email: k.anderson@beatson.gla.ac.uk Tel +44 141 330 2864

Abstract

Cancer invasion and metastasis occur in a complex three-dimensional environment, with reciprocal feedback from the surrounding host tissue and vasculature governing behavior. In this study, we used a novel intravital method that revealed spatiotemporal regulation of Src activity in response to the anti-invasive Src inhibitor dasatinib. A FLIM-FRET Src-biosensor was used to monitor drug targeting efficacy in a transgenic p53-mutant mouse model of pancreatic cancer. In contrast to conventional techniques, FLIM-FRET analysis allowed for accurate, time-dependent, live monitoring of drug efficacy and clearance in live tumors. In three-dimensional organotypic cultures, we demonstrated that a spatially distinct gradient of Src activity exists within invading tumor cells, governed by the depth of penetration into complex matrices. In parallel, this gradient was also found to exist within live tumors, where Src activity is enhanced at the invasive border relative to the tumor cortex. Upon treatment with dasatinib we observed a switch in activity at the invasive borders, correlating with impaired metastatic capacity in vivo. Src regulation was governed by the proximity of cells to the host vasculature, as cells distal to the vasculature were regulated differentially in response to drug treatment compared to cells proximal to the vasculature. Overall, our results in live tumors revealed that a threshold of drug penetrance exists *in vivo* and that this can be used to map areas of poor drug targeting efficiency within specific tumor microenvironments. We propose that employing FLIM-FRET in this capacity could provide a useful preclinical tool in animal models prior to clinical translation.

Introduction

Maximising the utility of preclinical disease models in drug discovery requires the development of new innovative approaches for the study of drug delivery at the molecular level in live tissue. Examining cancer behavior in an intact host setting allows us to understand, in a more physiological context, the aberrant regulation of critical events that drive tumor progression. Intravital imaging is providing new insights on how cells behave in a more native microenvironment, thereby improving our understanding of disease progression [1,2]. In combination with adaptations of *in vitro* molecular techniques to three-dimensional model systems, intravital imaging is helping to bridge the gap in our understanding of key biological events that govern cancer progression and therapeutic response *in vivo* [2,3,4].

Pancreatic ductal adenocarcinoma (PDAC) is one of the most lethal forms of human cancer, with 90% of patient deaths occurring within 1 year of diagnosis due to surgically unresectable, locally advanced or metastatic disease being present at the time of clinical diagnosis [5]. Systemic therapies are largely ineffective in inoperable disease, leading to an overall 5-year survival rate of less than 5% [6,7]. In addition, the tumor microenvironment is characterized by poor vascularity and extensive deposition of ECM, limiting the accumulation and perfusion of drug delivery within the tumor tissue [8,9,10]. Consequently, the development of more effective strategies to efficiently target and treat pancreatic cancer is required.

Recently we have used a genetically engineered (*Kras*$^{G12D/+}$; *Trp53*$^{R172H/+}$; *Pdx1-Cre* (KPC)) mouse model of pancreatic cancer in which Cre-lox technology is used to target Kras^{G12D} and mutant p53^{R172H} to the pancreas via the Pdx1 promoter [11]. This results in the formation of invasive and metastatic PDAC that recapitulates the pathology of human disease [12,13]. Using this model, we previously

demonstrated that introduction of a mutant $p53^{R172H}$ allele, drives a metastatic program, over and above the tumor-promoting effects of p53 loss [14]. We and others have also shown that mutations in p53 provide a gain-of-function role that drives metastasis, via disruption of cell-cell and cell-matrix adhesion, leading to invasion and spread of disease [14-20].

A number of new therapeutics have been developed to exploit the deregulation of non-receptor tyrosine kinases such as Src in cancer and are currently under clinical investigation [21]. Elevated expression and/or activity of Src has been shown to contribute to various types of invasive tumor cell behavior including evasion of apoptosis, enhancement of proliferation and the deregulation of cell-cell and cell-matrix adhesions, associated with numerous forms of cancer including pancreatic cancer [22-24]. In line with this, we recently demonstrated a correlation between Src up-regulation and activation with reduced survival in human pancreatic cancer, and showed that the level of Src and phospho-Src are important indicators of vascular invasion, lymph node positivity and prognosis in human PDAC [25]. Importantly, we also established that the small molecule Src kinase inhibitor, dasatinib, which is currently being clinically evaluated in combination with chemotherapy in locally advanced PDAC [26] inhibited invasion of primary PDAC cells generated from this model, and significantly reduced the development of metastases by ~50% [25].

As the current therapeutic failure of agents in the treatment of pancreatic cancer may arise from a potentially reversible impairment in drug delivery to the tumor [27] it remains to be determined whether improvements in drug targeting and effective delivery could enhance the encouraging anti-metastatic profile of dasatinib and improve survival in this aggressive disease [25].

Here, we have adopted a fluorescence resonance energy transfer (FRET) biosensor, previously used to examine the dynamic regulation and activation state of Src kinase *in vitro* [28] as a preclinical tool to assess drug delivery and efficacy in live tumors. Using fluorescence lifetime imaging microscopy (FLIM) to measure FRET, we have rapidly analyzed and quantitatively measured Src activity at a single/sub-cellular level *in vivo* and detected effects intractable to standard techniques. We have investigated aspects of the three-dimensional tumor environment that may contribute to poor drug targeting, such as the proximity of cells to the host vasculature or their location with regards to the tumor cell core or invasive border. Critically, we exploit this detailed spatial and temporal mapping of drug response to monitor the heterogeneity of tumor cells in response to new combination therapy that targets the stromal ECM architecture to favor effective drug delivery within solid tumor tissue.

Material and Methods

Cell culture. Primary mouse PDACs were derived from tumors harvested from *Pdx1-Cre-GFP, LSL-KRas$^{G12D/+}$, LSL-Trp53$^{R172H/+}$* mice [14]. PDACs were cultured in DMEM supplemented with 10% FBS and 2 mM L-glutamine (Invitrogen) and transfected with the ECFP-YPet Src-FRET biosensor using Polyfect as described by manufacturers protocol (Qiagen) [28]. Cells were selected using 0.6 mg/ml G418 and stable pools generated using standard procedures.

M**ultiphoton TCSPC FLIM**. Imaging was performed on a Nikon Eclipse TE2000-U inverted microscope with an Olympus long working distance 20x 0.95 NA water immersion lens. The excitation source used for all image acquisition was a Ti:Sapphire femto-second pulsed laser (Cameleon, Coherent UK), operating at 80 MHz and tuned to a wavelength of 830 nm. For more details, see supplementary information.

Fluorescence life-time imaging of Src-FRET Biosensor *in vivo*. Following trypsinization, $1x10^6$ cells were re-suspended in 100 µl HBSS (Invitrogen) and subcutaneously injected into the rear flank of a nude mouse. Tumors were allowed to develop for 7 days. Animals were kept in conventional animal facilities and all experiments were carried out in compliance with UK Home Office guidelines. To permit imaging, mice were terminally anaesthetized using an anesthetic combination of 1:1 hypnorm - H_2O + 1:1 hypnovel - H_2O. Following induction of anesthesia the subcutaneous tumor was surgically exposed and the mouse restrained on a 37ºC heated stage. Multiphoton excited FLIM measurements were performed *in vivo* using the system described above. Typical scan parameters were 150 x 150 µm field of

view over 512 x 512 pixels scanned at 400 Hz with the acquisition of 100 frames. The pixel dwell time was 5 µs with a total acquisition time of ~120 seconds. Typical laser power as measured at the sample plane was ~30 mW. It was found that PDAC cells expressing the Src biosensor could be imaged at depths of up to 150 µm in live tumor tissue. To visualize vasculature, quantum dots (Qtracker-655, Visen medical, USA) were tail vein injected into mice 10 min prior to imaging (10 µl in 190 µl HBSS). For control or drug treated tumor, at least 300 cells were measured. Columns, mean; error bars represent ± SE, P value by unpaired student's t-test.

Frequency domain FLIM. *In vitro* fluorescence Lifetime measurements were performed using a Lambert Instruments fluorescence attachment (LIFA) on a Nikon Eclipse TE 2000-U microscope equipped with a 60x objective and a filter block consisting of a 436/20 excitation filter, a T455LP dichroic mirror, and a 480/40 emission filter. For more details, see supplementary information.

Organotypic invasion assay. Organotypic asays were performed as described previously [36]. Briefly, ~$7.5x10^4$/ml primary human fibroblasts were embedded in a three-dimensional matrix of rat tail collagen I. Rat tail tendon collagen was prepared by extraction with 0.5 M acetic acid to a concentration of ~2 mg/ml. Detached, polymerized matrix (2.5 ml) in 35 mm petri dishes was allowed to contract for 6-8 days in complete media (DMEM, supplemented with 10% FCS, Invitrogen) until the fibroblasts had contracted the matrix to 1.5 cm diameter. Subsequently, $4x10^4$ Src biosensor-expressing PDAC cells were plated on top of the matrix in complete media and allowed to grow to confluence for 4-5 days. The matrix was then mounted on a metal grid and raised to the air/liquid interface resulting in the matrix being fed from

below with complete media that was changed every 2 days. After 6-8 days invasion, the cultures were imaged as described or fixed using 4% paraformaldehyde and processed for hematoxylin and eosin (H&E) staining. For drug treatment, 100 nM of dasatinib (BMS) was added to the media below the matrix during the 6-8 day period as described. For cyclopamine treatment, 2.5-10 μM was added directly after matrix detachment prior to contraction [32,40]. Representative images of at least 3 independent experiments are shown, total of 985 cells assessed by FLIM-FRET. Columns, mean; error bars represent ± SE, P value by unpaired Student's t-test.

Drug treatment *in vitro* and *in vivo*. Dasatinib (a kind gift from Bristol Myers Squibb) was administered daily by oral gavage in 80 mmol/L citrate buffer [10 mg/kg] or 100 nM *in vitro* [19,25,29]. Cyclopamine (LC laboratories, USA) was administered by oral gavage [25 mg/kg] [42] or 2.5-10 μM *in vitro*. PP1 (Sigma Aldrich) [10 μM] and EGF (R&D systems) [50 ng/ml] was used *in vitro*.

Collagen organisation measurements using grey-level co-occurrence matrix (GLCM) analysis. Using ImageJ, summed intensity projections were formed from raw 16-bit TIFF z-stacks of the collagen SHG data. Three 100 x 100 μm^2 regions of interest were selected to assess the collagen present. These sub-regions were saved for analysis using an in-house modified version of the UMB GLCM features plugin [http://arken.umb.no/~kkvaal/eamtexplorer/imagej_plugins.html]. The modifications made allow for looped operation of the plugin for a user defined number of neighbor index points and for 0°, 90°, 180° and 270° directions of comparison. This allows for the calculation of the average texture parameters for each image. The plug-in was sequentially applied to each 100 x 100 μm^2 region of interest. Once all the images were analysed, the normalised texture parameters (contrast, uniformity, correlation,

homogeneity and entropy) were calculated for each images and imported into GraphPad Prism (version 5.00 for Mac OS X, GraphPad Software, San Diego California USA, www.graphpad.com). The mean parameters were plotted (averaging over all four directions) along with the SEM against the neighbor index. Data are shown as points and dashed lines represent the non-linear bi-exponential fit to each data set [37].

Results

Generation of a FLIM-FRET-based genetic model of pancreatic cancer. To study the dynamic regulation of Src activity in pancreatic cancer *in vivo*, we first established primary PDAC cells from the *Pdx1-Cre; Kras*$^{G12D/+}$*; Trp53*$^{R172H/+}$ (KPC) mouse model [14]. Using these primary PDAC cells we generated stable cells expressing a ECFP-YPet variant of the Src-FRET biosensor [28]. The biosensor is composed of ECFP, an SH2 domain, a flexible linker and a Src substrate peptide derived from the c-Src substrate p130cas, linked to YPet (Fig1A). When the substrate is unphosphorylated the biosensor adopts a compact conformation in which the fluorophores are in close proximity, resulting in high FRET efficiency. Upon Src-induced phosphorylation, the substrate peptide binds to the SH2 domain and separates YPet from ECFP, thereby decreasing FRET (Fig1A) [28]. The loss of FRET upon Src activation is consistent with the intramolecular interaction of the phosphorylated substrate with the SH2 domain, and the subsequent change in FRET efficiency can be measured using fluorescent lifetime imaging of the donor fluorophore, ECFP (Fig1A,B). In the lifetime color maps, low basal Src activity is represented as blue, while high Src activity is represented as warm red/yellow colors, and areas with low signal-to-noise ratio in which lifetime measurements cannot be achieved are black (Fig1B). A critical advantage of this approach is that the biosensor allows us to visualize the dynamic and reversible equilibrium of Src activity within single cells in real-time. The resulting PDACs expressing the Src biosensor therefore serve as an excellent genetic and fluorescent model system to quantify the spatial and temporal regulation of Src activity in pancreatic cancer (Fig1A,B) [11,12,13].

Application of the Src biosensor to investigate drug targeting. To establish whether FLIM-FRET analysis of the Src biosensor could be utilized to rapidly and accurately distinguish subtle changes in Src activity in response to therapeutic intervention, PDAC cells were subjected to dasatinib treatment in culture. Cells were treated with 100 nM of dasatinib, a dose previously shown to be biologically effective in the KPC model [25] and the activity of Src within individual cells was determined using FLIM-FRET. Following 120 sec of FLIM acquisition, a distribution of fluorescent lifetimes was obtained, where a peak in lifetime within control cells was evident between 2.4-2.5 ns (Fig1C, grey). Dasatinib treatment induced a shift in this lifetime distribution, yielding a lower peak of 2.2-2.3 ns (Fig1C, pink and overlay, red). Using this shift in lifetime distribution peaks, we stratified these readouts and used a cut-off of > 2.35 ns to classify cells as 'active', while lifetimes of < 2.35 ns were classed as 'inactive' (Fig1C,D and supplementary FigS1). This enabled us to analyse the status of individual cells with respect to features of their environment, and capture behavior which would be masked by average measurements of fluorescence within a field of cells. We next performed rapid pharmacodynamic measurements of dasatinib efficacy in PDAC cells by generating a single cell, FLIM-FRET-based, dose-response curve (Fig2A) supported by standard western blotting (Fig2B). The ability to monitor Src activity on a single cell basis and the fast acquisition provided by multi-photon based FLIM [19] demonstrates the advantage and potential application of this technique as a dynamic, single cell biomarker for drug targeting studies.

Temporal monitoring of drug targeting using a FRET-biosensor. To determine whether the Src biosensor could be used to monitor fluctuations in target activity and

drug clearance in a time-dependent manner, we performed an *in vitro* washout experiment in which PDAC cells were subjected to 100 nM dasatinib for 30 mins, and subsequently monitored Src activity in response to dasatinib withdrawal using FLIM-FRET over 6 hrs. The efficacy of dasatinib treatment was demonstrated by a significant decrease in the fraction of Src-active cells upon dasatinib treatment (Fig2C, decreasing from 54.8 ± 3.7 % to 35.7 ± 6.9 %). Following washout, a rapid recovery in the fraction of Src-active cells was observed after 1hr, which peaked at 3hrs ($P = 0.014$) and subsequently returned towards control levels within 6 hrs (Fig2C). The capacity to track Src activity overtime *in vitro* prompted us to gauge whether we could use this approach to investigate temporal drug targeting and clearance under more functional and physiological conditions in live animal tumors.

Monitoring drug targeting and clearance in a live microenvironment using FLIM-FRET. We have previously used multiphoton-based FLIM to quantify protein activity at depths of ~150 μm within solid tumor tissue, providing a powerful tool to directly examine cancer progression *in situ* [19]. This allowed us to readily investigate cells surrounded by ECM, stroma and vasculature in a live setting upon drug treatment. Here, we subcutaneously injected mice with primary PDAC cells, and once tumors were established, subjected these mice to daily oral gavage of 10 mg/kg of dasatinib for 3 days (Fig3A). Inactivation of Src activity was evident under these conditions, as previously described [19,25,29]. After the final administration of dasatinib, Src activity was subsequently monitored using FLIM-FRET at time points of 1-2 hrs; 4-6 hrs; 16 hrs and 24 hrs post-treatment (see imaging regimen Fig3A). After the final dose of dasatinib, a rapid recovery of Src activity was observed, reaching a maximum at 16 hr post-drug treatment before returning to control levels

within 24 hrs (Fig3B-D, quantified in E, P = 0.021). The rapid recovery of Src activity to control levels as early as 4-6 hrs post-dasatinib (Fig3E) could potentially explain the partially ineffective targeting of pancreatic tumors we previously observed after a single daily oral dose of 10 mg/kg in dasatinib-treated KPC mice, which resulted in a reduction of metastasis of ~50% [25]. Our FLIM-FRET analysis suggests that treating mice more frequently to counteract this early recovery may warrant future investigation in this GEM model [25].

Spatial regulation of Src activity in tumor subpopulations in 3D. The *in vivo* fluorescent lifetime assessment of the Src biosensor (Fig3) represents single cell measurements taken from cells located throughout the tumor mass. The activity of proteins involved in cancer progression can, however, also be locally regulated by different environmental cues within tumor cell subpopulations such as areas of invasive borders or within hotspots in the tumor microenvironment. By adapting *in vitro* optical techniques, such as fluorescence recovery after photo-bleaching (FRAP) or photo-activation (PA) to *in vivo* applications, we have previously demonstrated context-dependent differences in protein behavior governed by local signals during cancer progression *in vivo* [29][30]. We therefore sought to determine whether FLIM-FRET could be utilized to monitor response to drug treatment in spatially distinct tumor subpopulations.

Complex three-dimensional matrices such as organotypic assays have been used to mimic cell-ECM interactions *in vivo* [31,32,33]. They offer a source of growth factors and appropriate integrin engagement, resulting in bidirectional signaling between tumor cells and the surrounding stromal fibroblasts during invasion (Fig4A and supplementary movies M1,2). We therefore employed organotypic

matrices as previously described [34,35,36] to provide a controlled platform for assessment of Src activity in invading tumor cells prior to *in vivo* analysis. Organotypic matrices consisting of human fibroblasts and rat tail fibrillar collagen I were established, which when exposed to an air-liquid interface induce a chemotactic gradient that allows overlayed PDAC cells to invade over time (Fig4A). Consistent with our recent *in vitro* and *in vivo* data [14,19,20,25] KPC derived PDACs expressing the Src reporter invaded into the matrix within 8 days (Fig4B). To investigate Src activity during different stages of invasion we measured activity at 20 μm intervals up to 120 μm within the matrix (Fig4C,D). Interestingly, the fraction of active Src cells increased in proportion to the depth invaded (Fig4D). This spatially distinct gradient of Src activity within invading tumor cell subpopulations, suggests that in a three-dimensional context, a switch in Src activity may be regulated by cues from within the local microenvironment during invasion.

Next, we assessed the response to dasatinib treatment of tumor subpopulations in the upper section of the organotypic matrix (0-40 μm) compared to those at depth (60-120 μm). Cells were allowed to invade for 6 days followed by dasatinib treatment for the last 2 days. The fraction of active Src cells in the upper section did not significantly change upon dasatinib treatment, while the fraction of active Src cells at depth was significantly reduced (Fig4E). This also correlated with a reduction in invasion after treatment (Fig4B and supplementary FigS2 [19,25]). It is therefore possible to use FLIM-FRET to visualise activity within spatially distinct subpopulations of tumor cells and gauge context- and site-specific drug targeting efficiencies during processes such as invasion. We therefore investigated Src activity in distinct regions within living solid tumors.

Spatial regulation of Src within distinct tumor microenvironments *in vivo*. We have previously shown that primary PDAC cells expressing mutant $p53^{R172H}$ form subcutaneous tumors with highly invasive borders, whereas cells in which p53 is deleted, form non-invasive, encapsulated tumors [19]. To identify distinct tumor regions we used features of the tissue stroma visualised using second harmonic generation (SHG) imaging. Central regions of the tumor were characterised by anisoptropic distribution of collagen fibres, while border regions were readily identified by isotropic organisation as previously described [37]. Grey-level co-ocurrence matrix (GLCM) analysis was used to distinguish between the tumor center and border based on features of the SHG collagen image (Supplementary Fig S3) [37]. In line with our results using organotypic matrices (Fig4), we observed that Src activity correlated with regions of invasion in mutant p53 PDACs *in vivo* (Fig5). In control treated PDAC tumors, cells within the tumor core were found to be predominantly inactive (Fig5A,C), while cells within invasive borders were predominantly active (Fig5B,C). Upon dasatinib treatment, the fraction of active Src cells within the tumor center did not significantly change (26.6 ± 15.7% versus 25.2 ± 1.8% of active cells). However, at the invasive border, a switch from a predominantly active to inactive state was observed (55.2 ± 5.7% versus 40.4 ± 2.7%). These results demonstrate that cells within different microenvironments have differential sensitivity to therapeutic treatment across the tumor population and that FLIM-FRET can potentially be used to map areas of drug targeting efficiency.

Drug delivery and targeting efficacy in live tumors is governed by proximity to vasculature. Poor vasculature or limited drug perfusion to tumor tissue is thought to play a critical role in drug delivery and efficacy [27]. As tumor cells which are

located in areas of poor drug exposure may recolonize or subsequently repopulate to form micro-metastases following treatment, it would be beneficial to identify regions of poor drug delivery within various solid tumor environments using FLIM-FRET. Next, we determined whether single cell analysis of Src activity could be used to assess the targeting of dasatinib with respect to the host vasculature.

Mice bearing primary PDAC tumors were generated as before and treated with 10 mg/kg of dasatinib for 3 days (Fig3A). Prior to FLIM-FRET imaging, quantum dots (Qtracker-655) were intravenously injected to act as a contrast agent to identify tumor vasculature (Fig6A and supplementary movie M3). This enabled us to analyze Src activity within four key zones: 0-25 μm, 25-50 μm, 50-100 μm and >100 μm from vasculature. Using this approach we found that a spatial distribution of Src activity exists in this context, in line with previous results (Fig4 and Fig5). Src activity increased in proportion to the distance from blood supply (Fig6C, control) and using FLIM-FRET analysis we could accurately measure the response to dasatanib treatment in this spatial setting. Src activity in cells proximal to blood supply (0-25 μm) was readily reduced in response to dasatinib, resulting in the predominant form of Src in cells being converted from an active to inactive state (Fig6C, < 25 μm ± dasatinib). A similar effect was observed within 25-50 μm from vasculature (Fig6C, 25-50 μm ± dasatinib), reaching a limiting threshold at 50-100 μm from the vasculature (Fig6C, 50-100 μm ± dasatinib). Critically, PDAC cells beyond 100 μm from vasculature were inefficiently targeted, such that dasatinib treatment increased the inactive pool by 15.6 % compared to control treated mice, but the predominant pool of cells remained in an active state (Fig6C, > 100 μm ± dasatinib). Utilizing this approach we can therefore measure the limitations of drug targeting *in vivo* and pinpoint areas (Fig5) or thresholds (Fig6) of non-targeting and

poor drug delivery in live tumor tissue. Applying this target validation technology with combination therapy aimed at improving drug delivery we could potentially document site-specific and time-dependent improvements in response to new therapeutic regimens.

Measuring the efficacy of combination therapy using FLIM-FRET *in vivo*. Targeting the tumor architecture to favor drug penetration has recently been employed to improve drug delivery in pancreatic cancer [27]. In particular, the role that tumor-associated matrix and stromal tissue plays in the perfusion deficit found in pancreatic cancer has been an active area of research [8,9,10][38][39]. In the KPC mouse described here, therapy to deplete the tumor-associated ECM using the hedgehog signaling inhibitor IP-926 increased tumor perfusion and the therapeutic index of chemotherapeutic agents within the pancreas, and increased the overall survival in these mice when used in combination with chemotherapy [10]. Moreover, the enzymatic depletion of the abundant ECM component, glycosaminoglycan hyaluronan, [40] by PEGPH20 has recently been shown to improve the intra-tumor delivery of chemotherapeutic agents *in vivo* [8,9]. These studies, in part, suggest that the current therapeutic failure of agents in the treatment of pancreatic cancer may arise from a potentially reversible impairment in tumor drug delivery. Combination therapy to disrupt the deposition of ECM and sensitize tumors prior to treatment may improve the current efficacy of dasatinib in this disease [8][9][10][41]. As proof-of-principle, we investigated whether targeting the tumor ECM using the hedgehog signaling inhibitor cyclopamine [42] prior to dasatinib treatment could improve drug delivery within the tumor tissue and examined whether FLIM-FRET could be used as a tool to accurately quantify and monitor the limitations of this process.

To assess whether cyclopamine treatment reduces ECM content [10] we initially subjected organotypic matrices to cyclopamine treatment during matrix formation. Treatment with cyclopamine led to a dose-dependent reduction in stromal fibroblast-driven collagen I contraction (Fig7A,B). Moreover, the fibrillar and cross-linked collagen I content in organotypic matrices was significantly reduced as quantified by SHG imaging (as previously described [43]) and grey-level co-ocurrence matrix (GLCM [37]) analysis respectively (Fig7C,D and supplementary FigS4 and movies M4,5). Next, we assessed whether cyclopamine alone had any effect on Src activity within PDAC cells *in vitro*. Following cyclopamine treatment ranging from 2.5 μM-20 μM, Src activity was unaffected as determined by FLIM-FRET and western blotting analysis (Fig 7E,F).

To assess the effects of cyclopamine *in vivo*, mice were injected subcutaneously with primary PDAC cells, and tumor were allowed to form before treatment with cylopamine alone for 3-days by oral gavage. Cyclopamine targeting of the stroma and ECM normalised the tumor microenvironment *in vivo* resulting in a loss of the spatial distribution of Src activity observed in relation to the vasculature (compare Fig7G - Fig6C, control). As cyclopamine treatment alone had no effect on Src activity in tumor cell *in vitro* (Fig7E,F), this suggests that targeting the tumor stroma *in vivo* can affect the activity of tumor cells indirectly via targeting environmental cues from the host surroundings such as ECM components.

Combination therapy using cyclopamine pre-treatment and dasatinib was then examined and target inhibition within three key zones from tumor vasculature (25-50 μm, 50-100 μm and >100 μm) was determined. At 25-50 μm from vasculature, there was a significant increase in the proportion of cells that switched to a predominantly inactive state upon cyclopamine + dasatinib treatment compared with dasatinib alone

(compare Fig6C dasatinib alone to Fig7H + cyclopamine, 25-50 μm). A small, though not significant improvement in drug targeting in cells at 50-100 μm was also observed upon cylopamine pre-treatment (compare Fig6C dasatinib alone to Fig7H + cyclopamine, 50-100 μm (inactive 59.05% ± 12.35 (SEM) versus 64.97% ± 16.51 (SEM), respectively P = 0.407). Importantly, the effect of cyclopamine + dasatinib at 100 μm from the vasculature was equivalent to cyclopamine alone at this distance (Fig 7G). Indicating that we have reached the limitation of this combination therapy as no further improvement in drug efficacy at this distance can be achieved using this combination. As cyclopamine was shown to have no direct effect on Src activity in tumor cells alone (Fig 7E,F) this suggests that indirectly targeting the tumor architecture can effect Src activity within tumor cells. The capacity to monitor spatial regulation of protein species using FLIM-FRET technology can therefore be used as a tool to determine the boundaries of combination therapy and allow for improved targeting and therapeutic outcome in preclinical models within the limitations of the tissue microenvironment of interest.

Discussion

To improve upon the current high attrition rates and late stage failure in drug development, more innovative and informative approaches to candidate drug selection and clinical design are required [44]. Failure to translate drug candidates into clinical benefit suggest that conventional early drug discovery strategies and preclinical models are sub-optimal and may poorly predict the heterogeneous drug response to effectively guide clinical dosing or combination strategies [45].

Here we demonstrate the utility of FLIM-FRET in the preclinical analysis of a dynamic biomarker *in vivo* during the assessment of therapeutic drug treatment. Detailed topological analysis at cellular and subcellular resolution in live tumor tissue has enabled precise detection and single cell quantification of subtle changes in protein activity over time that cannot faithfully be achieved using standard fixed endpoint approaches applied to *in vitro* cultured models or ex-vivo immunohistochemical analysis [2,44]. Using a genetically engineered model of pancreatic cancer that recapitulates the human disease and a novel therapeutic with demonstrated activity in pancreatic cancer, we have quantified the improvement in drug response associated with combination therapy and illustrate the application and advantages of FLIM-FRET in the drug target validation process. The distinct spatial- and environment-based regulation of Src observed here raises the possibility that other cancer types may harbor inefficiently targeted regions governed by unique microenvironments found within the local tumor tissue. Combination of preclinical mouse models with the rapidly expanding portfolio of new FRET-based biosensors [46,47,48,49] could prove useful for assessing the response to therapy of a wide variety of potential drug targets. Furthermore, intravital FLIM-FRET imaging could

provide a pixel-by-pixel map of protein activity in response to drug targeting in other forms of cancer or disease states.

Advances in systems biology approaches to drug discovery consider the complexity of disease and offer alternative strategies for target selection, validation and drug profiling [44,45]. In the fluorescence lifetime imaging field, advances have led to high-speed FLIM being developed to monitor protein activity or protein-protein interactions *in vitro* in a format suitable for high-content chemical or molecular screening [44][50]. Both time domain or frequency domain based-FLIM have been adapted to allow for fast FLIM in a 96-well high-throughput platform and as such have permitted a multiplexed FRET-readout of distinct and independent protein species that can be temporally and spatially resolved *in vitro* [51,52]. This, along with recent work using FLIM to identify tyrosine phosphorylation networks in response to EGFR signaling in a high throughput setting [53] highlights the potential application of FLIM for resolving transient compensatory and adaptive signaling events in response to a variety of drug treatment regimens. Early employment of FLIM-FRET imaging to intermediate three-dimensional and *in vivo* setting, as described here, may reveal further layers and context-dependent detail regarding drug response not feasible *in vitro* [54].

Finally, the dynamic tumor analysis described here can be applied to other strategies aimed at altering drug delivery, such as approaches to enhance the vascular patency of blood vessels prior to treatment to increase perfusion within the tumor tissue [8,9]. The transient normalization of tumor vessels in response to short-term anti-angiogenic agents has also been shown to temporarily enhance drug delivery to tumors [55]. There is therefore a clear limit to how much we can alter the ECM or blood supply, such that we do not compromise the integrity and structure of the

organ/tissue of interest. Use of this imaging technology with combination therapy may help determine the appropriate therapeutic window for altering the equilibrium between the tumor tissue and microenvironment, while maintaining maximum drug delivery (supplementary FigS5). Lastly, the intravital imaging approach applied in this study to assess protein behavior can also be applied in other biological frameworks where heterogeneity may determine therapeutic response, thereby assisting in the design, scheduling and streamlining of efficient drug delivery in a wide variety of disease conditions.

Acknowledgements

The authors thank Dr H. Bennett for critical reading of the manuscript and D. Miller, T. Hamilton, C. Nixon, M. O'Prey, T. Gilbey and D. Strachan for their expertise. This project was funded by CRUK core grant and P. Timpson by ARC, NHMRC and CINSW.

References

1. Weissleder R, Pittet MJ (2008) Imaging in the era of molecular oncology. Nature 452: 580-589.
2. Timpson P, McGhee EJ, Anderson KI (2011) Imaging molecular dynamics in vivo--from cell biology to animal models. Journal of cell science 124: 2877-2890.
3. Giepmans BN, Adams SR, Ellisman MH, Tsien RY (2006) The fluorescent toolbox for assessing protein location and function. Science 312: 217-224.
4. Beerling E, Ritsma L, Vrisekoop N, Derksen PW, van Rheenen J (2011) Intravital microscopy: new insights into metastasis of tumors. Journal of cell science 124: 299-310.
5. Li D, Xie K, Wolff R, Abbruzzese JL (2004) Pancreatic cancer. Lancet 363: 1049-1057.
6. Jensen OM, Esteve J, Moller H, Renard H (1990) Cancer in the European Community and its member states. Eur J Cancer 26: 1167-1256.
7. Warshaw AL, Fernandez-del Castillo C (1992) Pancreatic carcinoma. N Engl J Med 326: 455-465.
8. Jacobetz MA, Chan DS, Neesse A, Bapiro TE, Cook N, et al. (2012) Hyaluronan impairs vascular function and drug delivery in a mouse model of pancreatic cancer. Gut.
9. Provenzano PP, Cuevas C, Chang AE, Goel VK, Von Hoff DD, et al. (2012) Enzymatic targeting of the stroma ablates physical barriers to treatment of pancreatic ductal adenocarcinoma. Cancer cell 21: 418-429.
10. Olive KP, Jacobetz MA, Davidson CJ, Gopinathan A, McIntyre D, et al. (2009) Inhibition of Hedgehog signaling enhances delivery of chemotherapy in a mouse model of pancreatic cancer. Science 324: 1457-1461.
11. Hingorani SR, Wang L, Multani AS, Combs C, Deramaudt TB, et al. (2005) Trp53R172H and KrasG12D cooperate to promote chromosomal instability and widely metastatic pancreatic ductal adenocarcinoma in mice. Cancer Cell 7: 469-483.
12. Olive KP, Tuveson DA (2006) The use of targeted mouse models for preclinical testing of novel cancer therapeutics. Clin Cancer Res 12: 5277-5287.
13. Hruban RH, Adsay NV, Albores-Saavedra J, Anver MR, Biankin AV, et al. (2006) Pathology of genetically engineered mouse models of pancreatic exocrine cancer: consensus report and recommendations. Cancer Res 66: 95-106.
14. Morton JP, Timpson P, Karim SA, Ridgway RA, Athineos D, et al. (2010) Mutant p53 drives metastasis and overcomes growth arrest/senescence in pancreatic cancer. Proceedings of the National Academy of Sciences of the United States of America 107: 246-251.
15. Muller PA, Vousden KH, Norman JC (2011) p53 and its mutants in tumor cell migration and invasion. The Journal of cell biology 192: 209-218.
16. Adorno M, Cordenonsi M, Montagner M, Dupont S, Wong C, et al. (2009) A Mutant-p53/Smad complex opposes p63 to empower TGFbeta-induced metastasis. Cell 137: 87-98.

17. Girardini JE, Napoli M, Piazza S, Rustighi A, Marotta C, et al. (2011) A Pin1/mutant p53 axis promotes aggressiveness in breast cancer. Cancer cell 20: 79-91.
18. Muller PA, Caswell PT, Doyle B, Iwanicki MP, Tan EH, et al. (2009) Mutant p53 drives invasion by promoting integrin recycling. Cell 139: 1327-1341.
19. Timpson P, McGhee EJ, Morton JP, von Kriegsheim A, Schwarz JP, et al. (2011) Spatial regulation of RhoA activity during pancreatic cancer cell invasion driven by mutant p53. Cancer research 71: 747-757.
20. Muller PA, Trinidad AG, Timpson P, Morton JP, Zanivan S, et al. (2012) Mutant p53 enhances MET trafficking and signalling to drive cell scattering and invasion. Oncogene.
21. Brunton VG, Frame MC (2008) Src and focal adhesion kinase as therapeutic targets in cancer. Current opinion in pharmacology 8: 427-432.
22. Frame MC (2002) Src in cancer: deregulation and consequences for cell behaviour. Biochimica et biophysica acta 1602: 114-130.
23. Lutz MP, Esser IB, Flossmann-Kast BB, Vogelmann R, Luhrs H, et al. (1998) Overexpression and activation of the tyrosine kinase Src in human pancreatic carcinoma. Biochemical and biophysical research communications 243: 503-508.
24. Hakam A, Fang Q, Karl R, Coppola D (2003) Coexpression of IGF-1R and c-Src proteins in human pancreatic ductal adenocarcinoma. Digestive diseases and sciences 48: 1972-1978.
25. Morton JP, Karim SA, Graham K, Timpson P, Jamieson N, et al. (2010) Dasatinib inhibits the development of metastases in a mouse model of pancreatic ductal adenocarcinoma. Gastroenterology 139: 292-303.
26. Evans TRJ, Van Cutsem, E., Moore, M.J., Purvis, J.D., Strauss, L.C., Rock, E.P., Lee, J., Lin, C., Rosemurgy, A., Arena, F.P., Gara, M., Armstrong, E., O'Dwyer, P.J. (2012) Dasatinib combined with gemcitabine (Gem) in patients (pts) with locally advanced pancreatic adenocarcinoma (PaCa): Design of CA180-375, a placebo-controlled, randomized, double-blind phase II trial. . Journal of Clin Oncol 30 (suppl), abs TPS4134.
27. Yu M, Tannock IF (2012) Targeting tumor architecture to favor drug penetration: a new weapon to combat chemoresistance in pancreatic cancer? Cancer cell 21: 327-329.
28. Wang Y, Botvinick EL, Zhao Y, Berns MW, Usami S, et al. (2005) Visualizing the mechanical activation of Src. Nature 434: 1040-1045.
29. Serrels A, Timpson P, Canel M, Schwarz JP, Carragher NO, et al. (2009) Real-time study of E-cadherin and membrane dynamics in living animals: implications for disease modeling and drug development. Cancer research 69: 2714-2719.
30. Canel M, Serrels A, Miller D, Timpson P, Serrels B, et al. (2010) Quantitative in vivo imaging of the effects of inhibiting integrin signaling via Src and FAK on cancer cell movement: effects on E-cadherin dynamics. Cancer research 70: 9413-9422.
31. Cukierman E, Pankov R, Stevens DR, Yamada KM (2001) Taking cell-matrix adhesions to the third dimension. Science 294: 1708-1712.
32. Timpson P, McGhee EJ, Erami Z, Nobis M, Quinn JA, et al. (2011) Organotypic collagen I assay: a malleable platform to assess cell behaviour in a 3-dimensional context. Journal of visualized experiments : JoVE: e3089.

33. Yamada KM, Cukierman E (2007) Modeling tissue morphogenesis and cancer in 3D. Cell 130: 601-610.
34. Dozynkiewicz MA, Jamieson NB, Macpherson I, Grindlay J, van den Berghe PV, et al. (2012) Rab25 and CLIC3 collaborate to promote integrin recycling from late endosomes/lysosomes and drive cancer progression. Developmental cell 22: 131-145.
35. Lindsay CR, Lawn S, Campbell AD, Faller WJ, Rambow F, et al. (2011) P-Rex1 is required for efficient melanoblast migration and melanoma metastasis. Nature communications 2: 555.
36. Dawson JC, Timpson P, Kalna G, Machesky LM (2012) Mtss1 regulates epidermal growth factor signaling in head and neck squamous carcinoma cells. Oncogene 31: 1781-1793.
37. Cicchi R, Kapsokalyvas D, De Giorgi V, Maio V, Van Wiechen A, et al. (2010) Scoring of collagen organization in healthy and diseased human dermis by multiphoton microscopy. Journal of biophotonics 3: 34-43.
38. Olson P, Chu GC, Perry SR, Nolan-Stevaux O, Hanahan D (2011) Imaging guided trials of the angiogenesis inhibitor sunitinib in mouse models predict efficacy in pancreatic neuroendocrine but not ductal carcinoma. Proceedings of the National Academy of Sciences of the United States of America 108: E1275-1284.
39. Komar G, Kauhanen S, Liukko K, Seppanen M, Kajander S, et al. (2009) Decreased blood flow with increased metabolic activity: a novel sign of pancreatic tumor aggressiveness. Clinical cancer research : an official journal of the American Association for Cancer Research 15: 5511-5517.
40. Edward M, Gillan C, Micha D, Tammi RH (2005) Tumour regulation of fibroblast hyaluronan expression: a mechanism to facilitate tumour growth and invasion. Carcinogenesis 26: 1215-1223.
41. Brekken C, de Lange Davies C (1998) Hyaluronidase reduces the interstitial fluid pressure in solid tumours in a non-linear concentration-dependent manner. Cancer letters 131: 65-70.
42. Thayer SP, di Magliano MP, Heiser PW, Nielsen CM, Roberts DJ, et al. (2003) Hedgehog is an early and late mediator of pancreatic cancer tumorigenesis. Nature 425: 851-856.
43. Samuel MS, Lopez JI, McGhee EJ, Croft DR, Strachan D, et al. (2011) Actomyosin-mediated cellular tension drives increased tissue stiffness and beta-catenin activation to induce epidermal hyperplasia and tumor growth. Cancer cell 19: 776-791.
44. Isherwood B, Timpson, P, Mcghee, E.J , Anderson, K.I , Canel, M , Serrels, A , Brunton, V.G , Carragher, N.O. (2011) Live cell in vitro and in vivo imaging applications: Accelerating drug discovery. Pharmaceutics 3: 141-170.
45. Kamb A (2005) What's wrong with our cancer models? Nat Rev Drug Discov 4: 161-165.
46. Festy F, Ameer-Beg SM, Ng T, Suhling K (2007) Imaging proteins in vivo using fluorescence lifetime microscopy. Mol Biosyst 3: 381-391.
47. Wouters FS, Verveer PJ, Bastiaens PI (2001) Imaging biochemistry inside cells. Trends Cell Biol 11: 203-211.
48. Dehmelt L, Bastiaens PI (2010) Spatial organization of intracellular communication: insights from imaging. Nat Rev Mol Cell Biol 11: 440-452.

49. Seong J, Ouyang M, Kim T, Sun J, Wen PC, et al. (2011) Detection of focal adhesion kinase activation at membrane microdomains by fluorescence resonance energy transfer. Nature communications 2: 406.
50. Talbot CB, McGinty J, Grant DM, McGhee EJ, Owen DM, et al. (2008) High speed unsupervised fluorescence lifetime imaging confocal multiwell plate reader for high content analysis. Journal of biophotonics 1: 514-521.
51. Grant DM, Zhang W, McGhee EJ, Bunney TD, Talbot CB, et al. (2008) Multiplexed FRET to image multiple signaling events in live cells. Biophys J 95: L69-71.
52. Kumar S, Alibhai D, Margineanu A, Laine R, Kennedy G, et al. (2011) FLIM FRET technology for drug discovery: automated multiwell-plate high-content analysis, multiplexed readouts and application in situ. Chemphyschem : a European journal of chemical physics and physical chemistry 12: 609-626.
53. Grecco HE, Roda-Navarro P, Girod A, Hou J, Frahm T, et al. (2010) In situ analysis of tyrosine phosphorylation networks by FLIM on cell arrays. Nat Methods 7: 467-472.
54. Bakker GJ, Andresen V, Hoffman RM, Friedl P (2012) Fluorescence lifetime microscopy of tumor cell invasion, drug delivery, and cytotoxicity. Methods in enzymology 504: 109-125.
55. Jain RK (2005) Normalization of tumor vasculature: an emerging concept in antiangiogenic therapy. Science 307: 58-62.

Figure 1. Utility and characterization of Src-biosensor for monitoring drug targeting. A, Schematic of multiphoton based FLIM-FRET acquisition of the ECFP-YPet reversible Src-biosensor upon the activity of Src kinase or phosphatases, adapted from [28] B, Representative fluorescence image of ((KPC) $Kras^{G12D}$; $p53^{R172H}$; Pdx1Cre)[11] derived primary PDAC cells expressing the Src-biosensor (green) with corresponding lifetime maps of Src activity ± 100 μM dasatinib. C, D Quantification and distribution of fluorescent lifetime in response to 100 nM dasatinib treatment for 2 hrs. Stratified readouts from the Src biosensor were utilized as a threshold for cells being classified as 'active' lifetimes > 2.35 ns or 'inactive' lifetimes < 2.35 ns, based on the distribution between pre/post treatment peaks (arrow heads). Grey = control, pink = dasatinib, red = overlay. Columns, mean; bars, SE. **, P = 0.0001 by unpaired Student's t-test.

Figure 2. Application of FLIM-FRET for rapid and dynamic drug targeting studies. A, Quantification and distribution of Src-biosensor lifetime measurements in response to increasing concentrations of dasatinib, ranging from 5 nM to 200 nM (left hand panel). FLIM-FRET generated dose-response curve to dasatinib treatment *in vitro* (right hand panel). B, Corresponding western blot assessment of Src autophosporylation using anti-phospho-Src Y416, -Src and -actin antibodies respectively in response to dasatinib treatment for 2 hrs. C, Single cell FLIM-FRET quantification permitting the detailed tracking of fluctuations in active/inactive fraction of Src following pre-treatment and subsequent washout of 100 nM dasatinib over a 6 hr time period. Columns, mean; bars, SE. *, P = 0.036; **, P = 0.041; ***, P = 0.014 and ****, P = 0.006 by unpaired Student's t-test.

Figure 3. Monitoring drug targeting efficacy and clearance in a live tumor microenvironment using Src biosensor. A, Schematic depicting drug treatment and *in vivo* FLIM-FRET imaging regimen. After 7 days of tumor development, dasatinib was administered at 10 mg/kg by oral gavage once daily for 3 days. Upon the last administration of dasatinib, four post administration lifetime measurements of Src activity were obtained using *in vivo* FLIM-FRET analysis, ranging from; 1-2, 4-6, 16 and 24 hrs post-treatment. B-D, Representative *in vivo* fluorescence images of PDACs expressing the Src-reporter (green) with SHG signal from host ECM components (purple) at 1-2 hrs (left hand panels), 4-6 hrs (middle panels) and 24 hrs (right hand panels), post-oral administration of dasatinib. Corresponding *in vivo* lifetime maps (lower panels), demonstrating the capacity to monitor single cell fluctuations in the fraction of active/inactive cells over the time course of dasatinib treatment in live tumor tissue. Red arrows depict active tumor subpopulation, white arrows depict inactive cells. E, Quantitative FLIM-FRET imaging post-dasatinib treatment (1-2, 4-6, 16 and 24 hrs), demonstrates the capacity to quantify fluctuations and the distribution in drug target activity over time in a live tumor environment. Columns, mean; bars, SE. *, $P = 0.037$; ** $P = 0.025$ and *** $P = 0.021$ by unpaired Student's t-test.

Figure 4. Spatial regulation of Src activity within 3D-tumor subpopulations. A, Primary PDAC cells (green) interacting with stromal fibroblasts (red) and SHG signal from collagen I (purple) during three-dimensional invasion on organotypic matrix over 8 days. White arrow head (right hand z-projection panel) indicates interactions between co-cultured tumor cells and fibroblasts. B, H&E-stained sections of PDAC cell invasion after 6 days ± 2 days post-invasion dasatinib treatment. C,

Corresponding lifetime map of Src activity in PDAC cells in upper section of matrix (0-40 μm) or at depth within the matrix (60-120 μm). D, Quantification of lifetime measurements of Src activity at distinct depths within the matrix ranging from the surface at 0 μm to 120 μm within the matrix, in intervals of 20 μm. E, Quantification of fluorescence lifetime measurements of Src activity in tumor subpopulations at the surface or within the matrix ± 100 nM dasatinib. The distribution of active and inactive cells within the top or bottom of the matrix are expressed (%) of total tumor tissue population. Columns, mean; bars, SE. *, P = 0.027; **, P = 0.021; ***, P = 0.006 and ****, P = 0.001 by unpaired Student's t-test.

Figure 5. Src activity is subject to spatial regulation within tumor subpopulations in live tumor microenvironments. A,B Representative *in vivo* fluorescence images of PDAC cells (left hand panels) expressing the Src-reporter (green) with SHG signal from host ECM components (purple). Corresponding *in vivo* lifetime maps (right hand panels) demonstrating the distinct activation state of Src within the tumor center or invasive border ± 10 mg/kg oral administration of dasatinib (white dashed lines indicate position of invasive border). C, *In vivo* quantification of the activation state of cells (%) population within distinct regions of the tumor environment ± 10mg/kg dasatinib. Columns, mean; bars, SE.*, P = 0.04 by unpaired Student's t-test.

Figure 6. Quantification of drug delivery *in vivo* with respect to tumor vasculature using FLIM-FRET. A, Representative *in vivo* fluorescence image of PDAC cells expressing the Src-biosensor (green) in the context of host tumor vasculature, labelled with Qtracker 655 quantum dots (red) and SHG signal from host ECM components (purple). Corresponding *in vivo* lifetime map demonstrates the capacity to monitor

distinct activation states of Src in the context of the drug perfusion from tumor blood supply. B, Representative *in vivo* fluorescence image of primary PDAC cells expressing the Src-biosensor (green) in context of host vasculature (red) with corresponding *in vivo* lifetime map in the presence of 10 mg/kg dasatinib treatment. Vascular imaging regimen determining the proximity of cells to the local vasculature within four key zones including; 0-25 μm, 25-50 μm, 50-100 μm and > 100 μm from blood supply. C, *In vivo* quantification of Src targeting activity in the context of tumor blood supply, demonstrating a spatially restricted propagation of Src inactivation upon 10 mg/kg oral administration of dasatinib. Columns, mean; bars, ± SE.

Figure 7. Combination therapy targeting stroma compartment improves drug delivery to solid tumors and targeting efficiency can be monitored using intravital FLIM-FRET imaging. A,B, Representative image and quantification of fibroblast-induced organotypic ECM remodelling and contraction ± increasing dose of cyclopamine (0-10 μM). C, Representative maximum SHG-projection image of organotypic fibrillar collagen I ECM content (purple) ± 10 μM cyclopamine. D, Z-stack quantification (0-80 μm) of SHG-based fibrillar collagen I content ± 10 μM cyclopamine as described previously [43]. E, *In vitro* quantification of Src activity ± cyclopamine treatment (0-10 μM) using FLIM-FRET. F, *In vitro* Western blot analysis of Src activity ± cyclopamine treatment (0-10 μM) using anti-phospho-Src Y416, Src and actin antibodies respectively. G,H FLIM-FRET quantification documenting site-specific changes in Src response to new combination treatment regimen (50 μm resolution). Columns, mean; bars, ± SE.

Figure 1

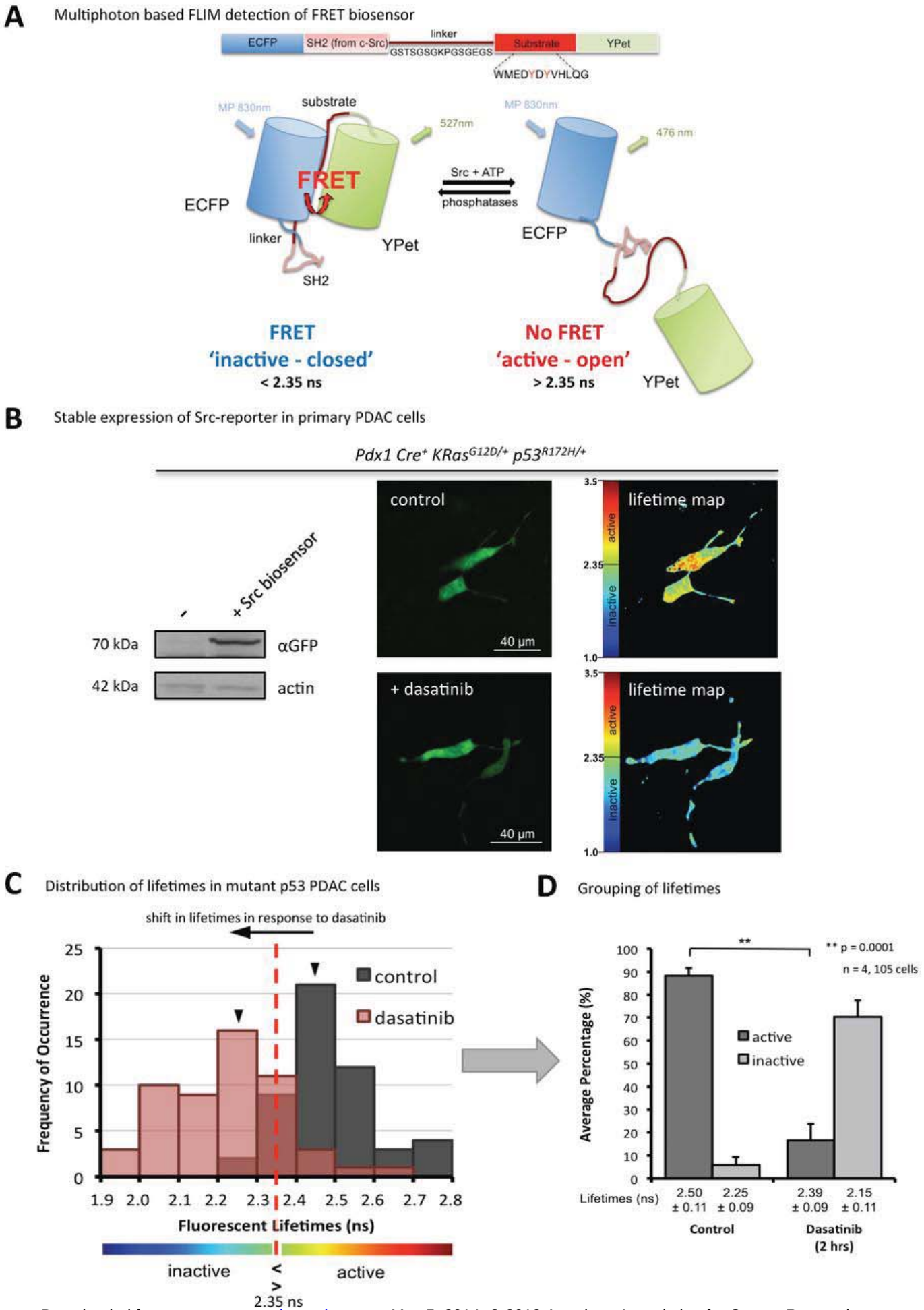

Figure 2

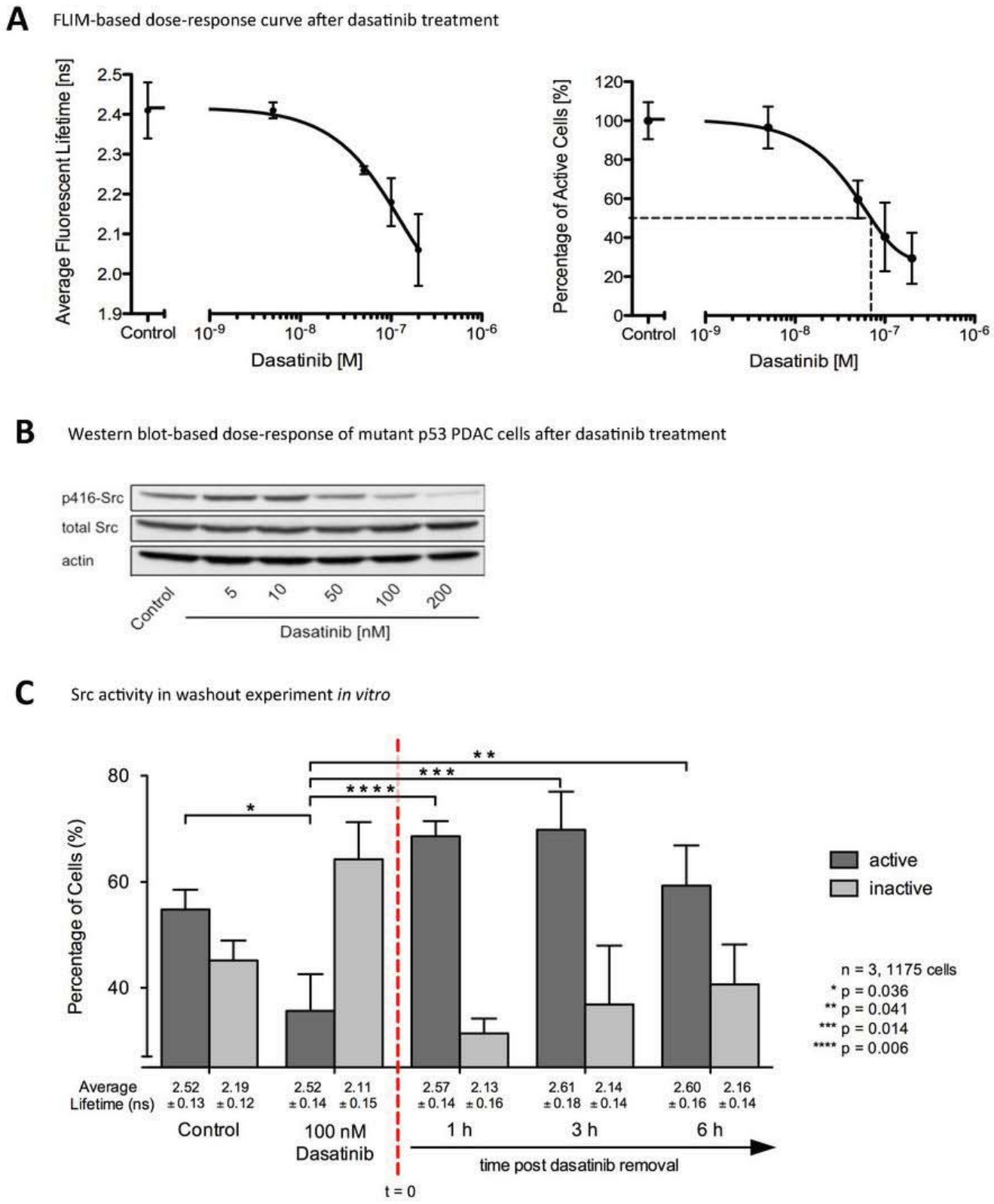

Figure 3

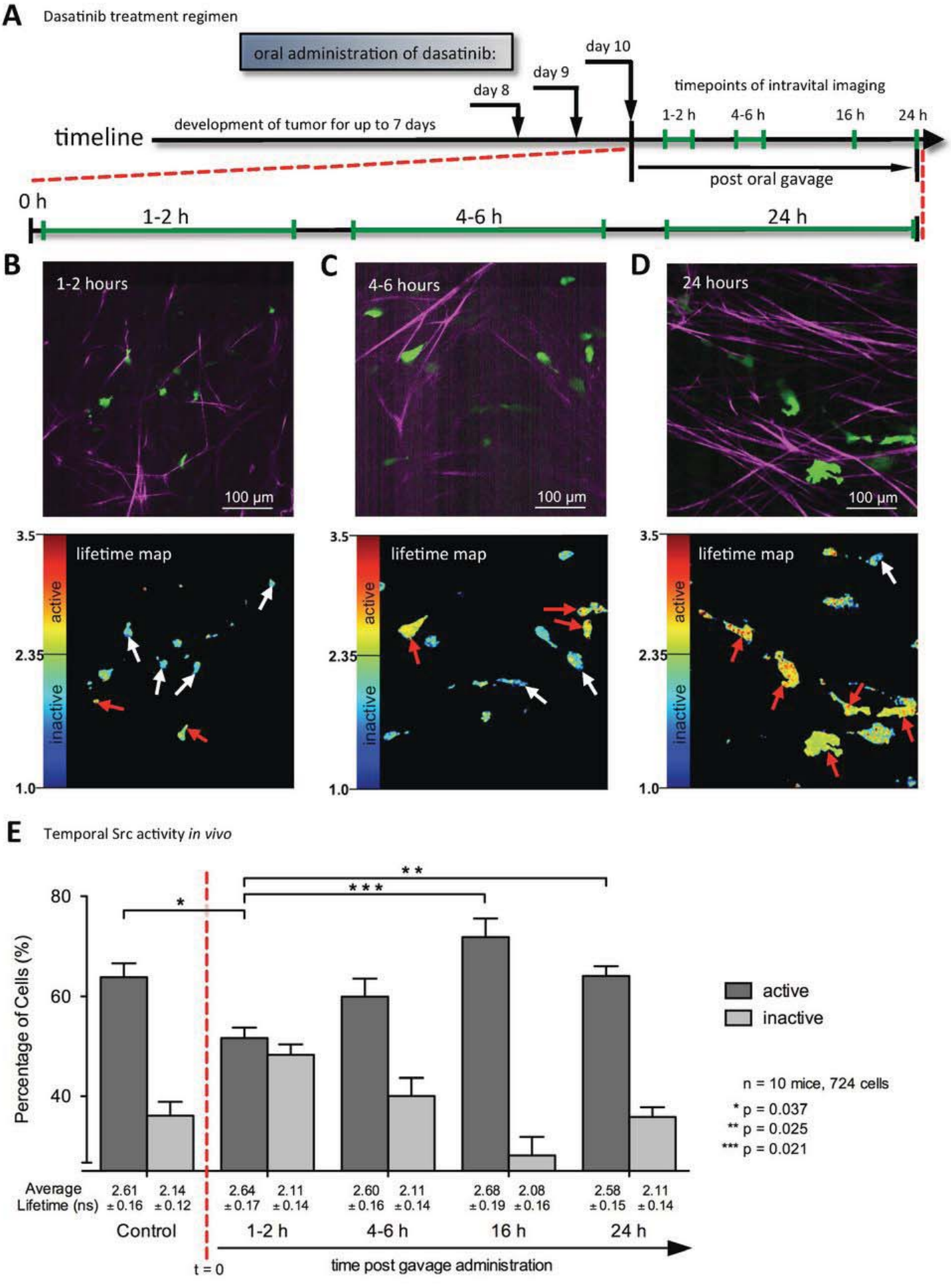

Author Manuscript Published OnlineFirst on June 7, 2013; DOI: 10.1158/0008-5472.CAN-12-4545
Author manuscripts have been peer reviewed and accepted for publication but have not yet been edited.

Figure 4

A Mutant p53 PDAC cells invading on an organotypic matrix

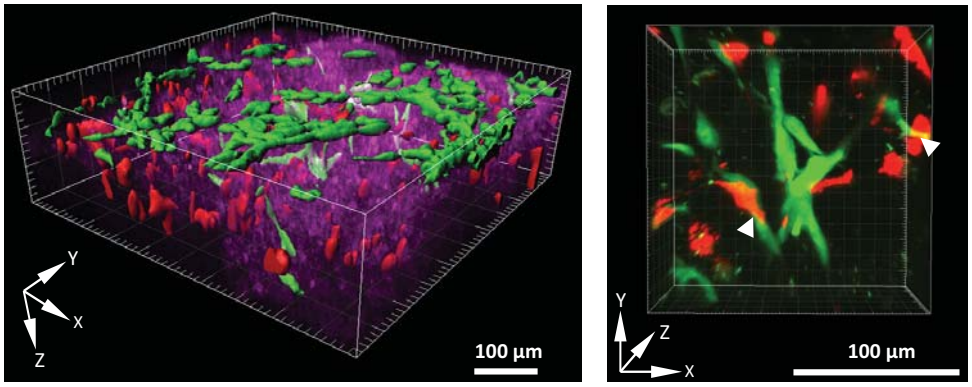

B Sections of invasion in organotypic matrices

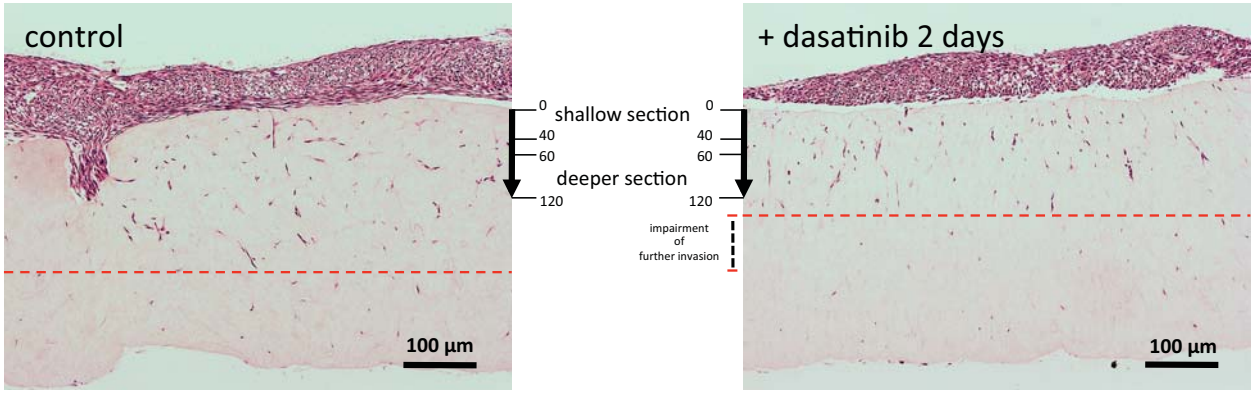

C Src activity in organotypic matrices

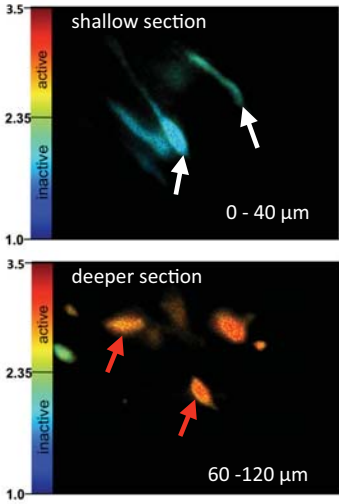

D Src activity in relation to depth penetrated into organotypic matrices

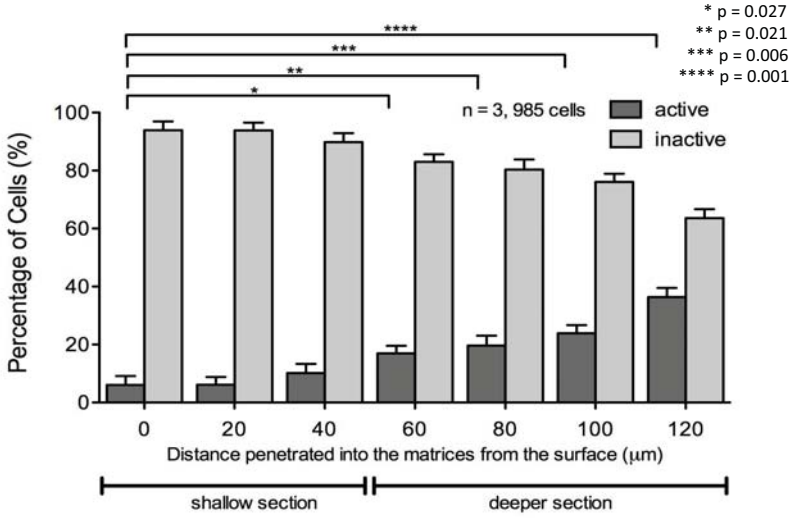

E Switch in distribution of Src activity after dasatinib treatment

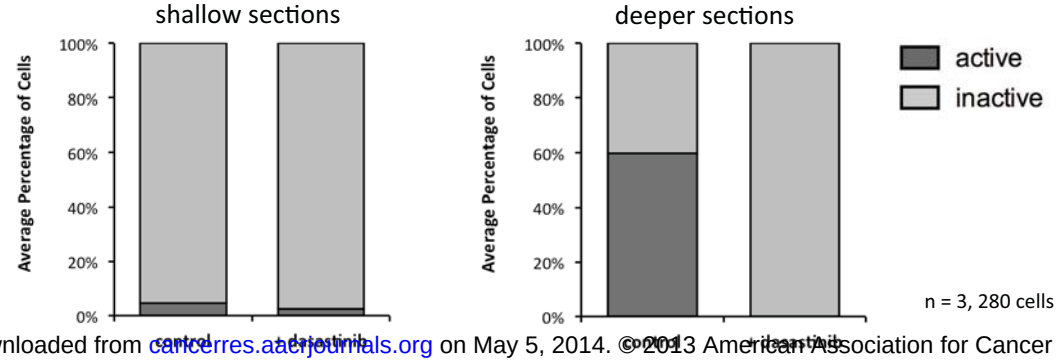

Figure 5

A Mutant p53 PDAC cells at the tumor core *in vivo*

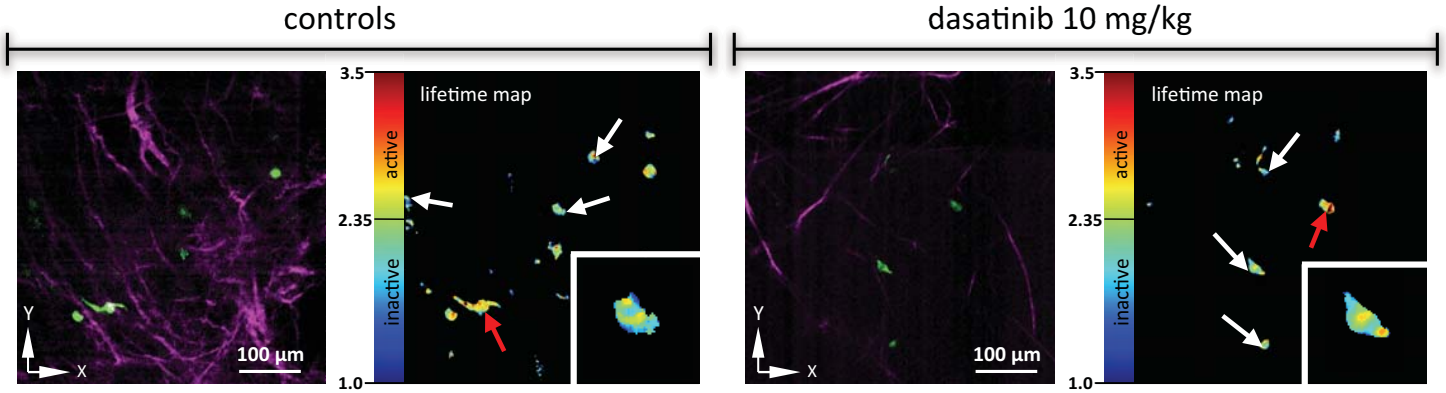

B Mutant p53 PDAC cells at the tumor border *in vivo*

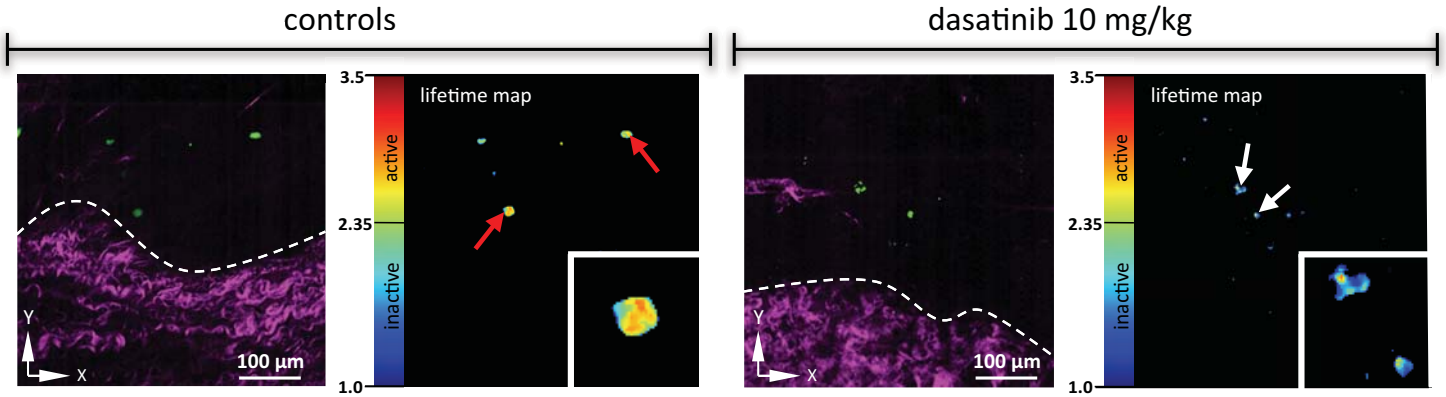

C Distribution of Src activity at the center and tumor border *in vivo*

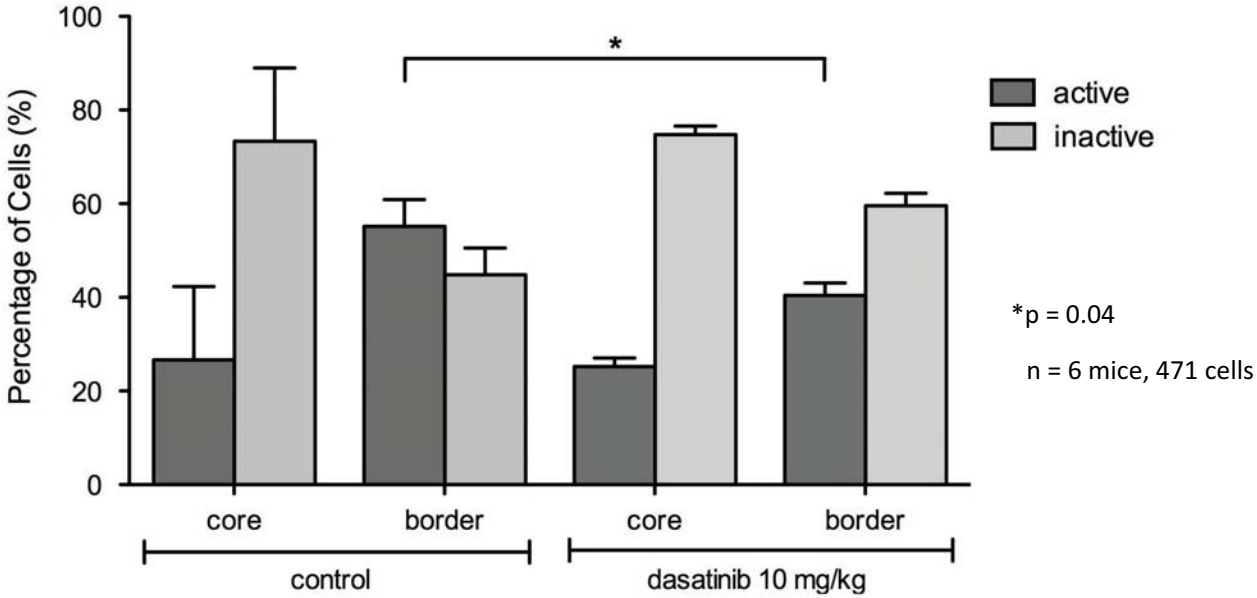

Author Manuscript Published OnlineFirst on June 7, 2013; DOI: 10.1158/0008-5472.CAN-12-4545
Author manuscripts have been peer reviewed and accepted for publication but have not yet been edited.

Figure 6

A Mutant p53 PDAC cells *in vivo* in context to vasculature

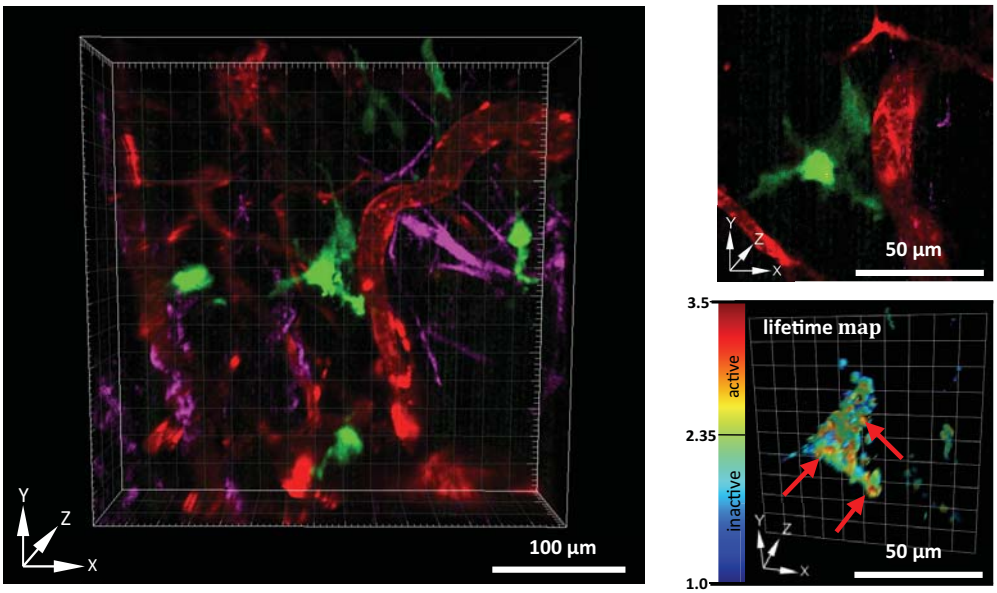

B Assessment of drug targeting in relation to tumour vasculature *in vivo*

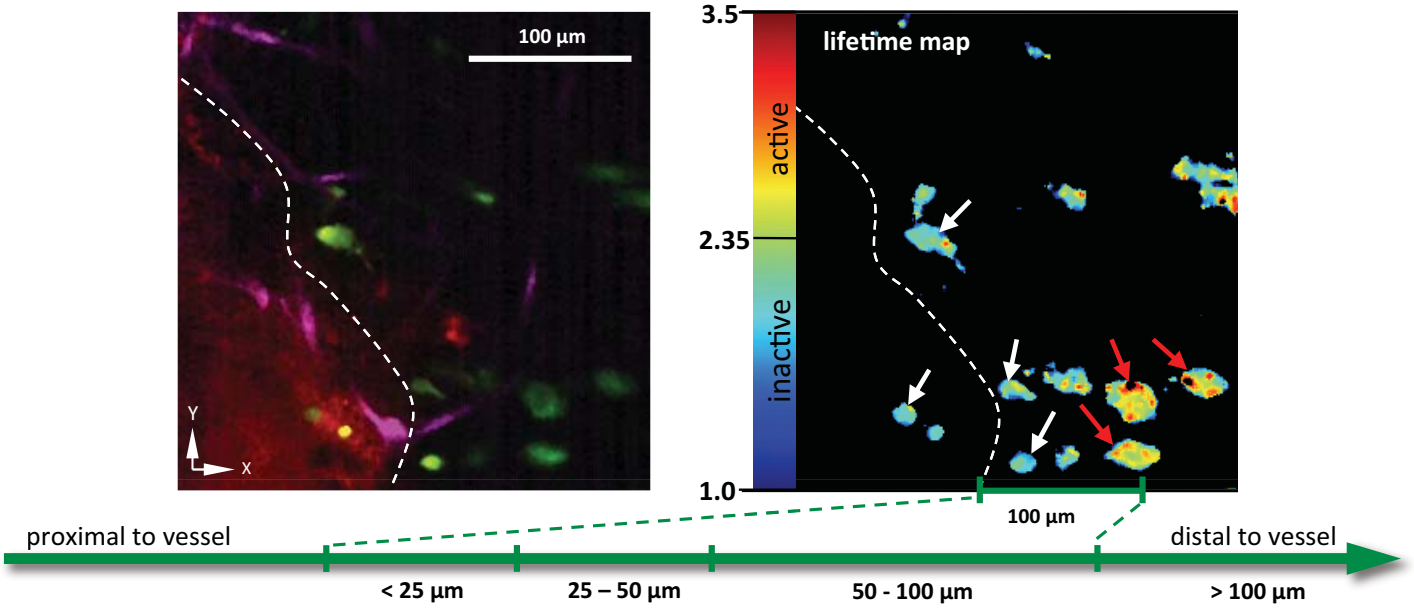

C Distribution of Src activity in relation to local vasculature *in vivo*

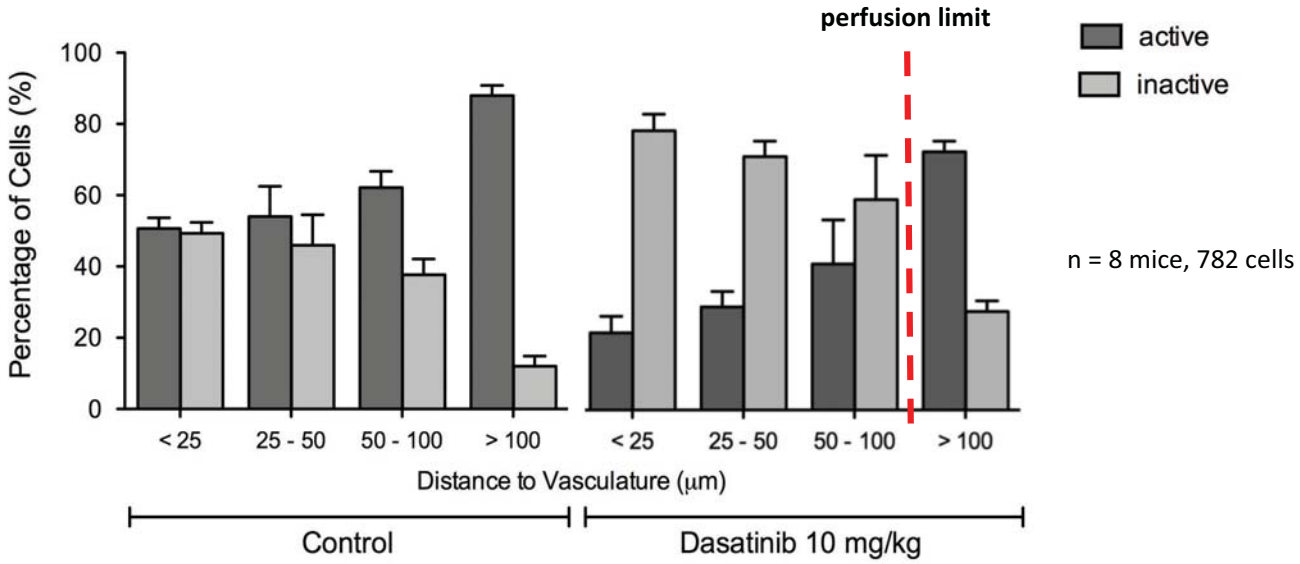

n = 8 mice, 782 cells

Author Manuscript Published OnlineFirst on June 7, 2013; DOI: 10.1158/0008-5472.CAN-12-4545
Author manuscripts have been peer reviewed and accepted for publication but have not yet been edited.

Figure 7

A Organotypic matrices after 6 days of contraction

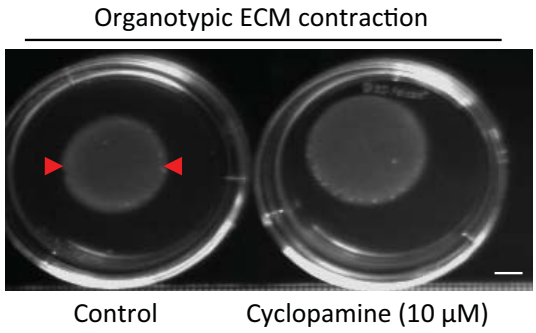

B Area of organotypic matrices

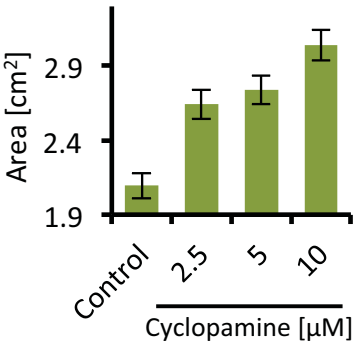

C Collagen detected by SHG after 6 days of contraction

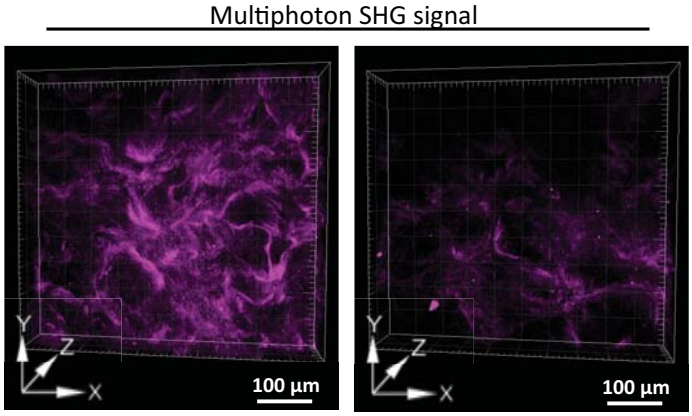

D Fibrillar collagen content in organotypic matrices

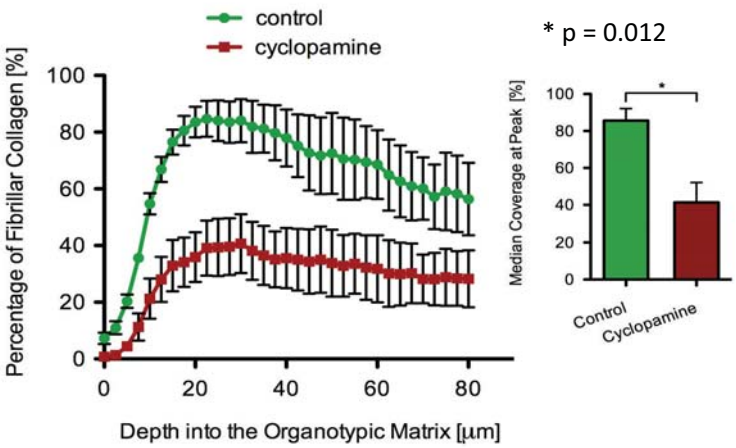

E FLIM-based response of mutant p53 PDAC cells to cyclopamine treatment *in vitro*

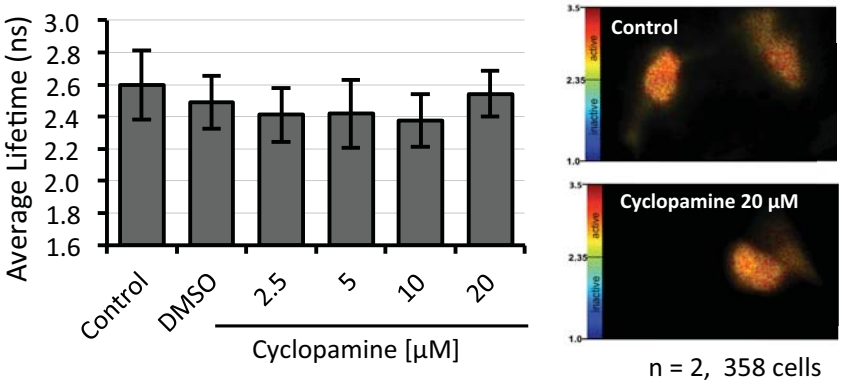

n = 2, 358 cells

F Western blot-based response to cyclopamine

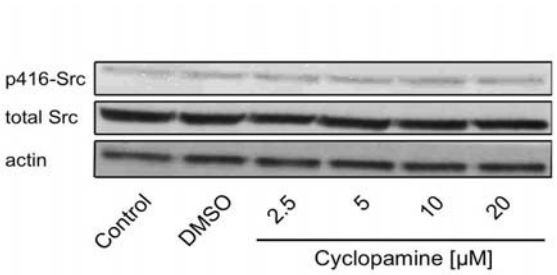

G Src activity in relation to local vasculature upon cyclopamine treatment *in vivo*

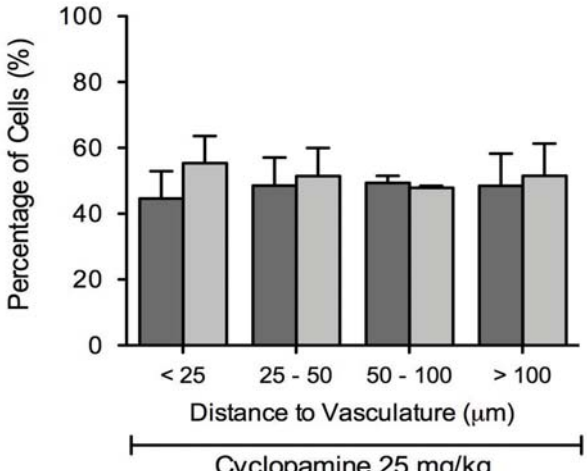

H Src activity in relation to local vasculature upon combination treatment *in vivo*

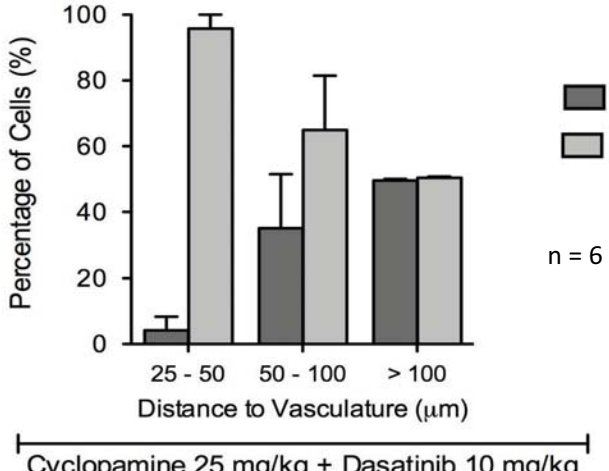

n = 6 mice, 364 cells